

Fragmentation functions at next-to-next-to-leading order accuracyDaniele P. Anderle^{*} and Marco Stratmann[†]*Institute for Theoretical Physics, University of Tübingen,
Auf der Morgenstelle 14, 72076 Tübingen, Germany*Felix Ringer[‡]*Theoretical Division, MS B283, Los Alamos National Laboratory, Los Alamos, New Mexico 87545, USA
and Institute for Theoretical Physics, University of Tübingen,
Auf der Morgenstelle 14, 72076 Tübingen, Germany*

(Received 21 October 2015; published 14 December 2015)

We present a first analysis of parton-to-pion fragmentation functions at next-to-next-to-leading order accuracy in QCD based on single-inclusive pion production in electron-positron annihilation. Special emphasis is put on the technical details necessary to perform the QCD scale evolution and cross section calculation in Mellin moment space. We demonstrate how the description of the data and the theoretical uncertainties are improved when next-to-next-to-leading order QCD corrections are included.

DOI: [10.1103/PhysRevD.92.114017](https://doi.org/10.1103/PhysRevD.92.114017)

PACS numbers: 13.87.Fh, 13.85.Ni, 12.38.Bx

I. INTRODUCTION AND MOTIVATION

Within the framework of perturbative QCD (pQCD), cross sections may be written in terms of perturbatively calculable hard-scattering coefficient functions convoluted with appropriate sets of nonperturbative but universal input functions constrained by data. The underlying theoretical foundations have been established in factorization theorems [1]. In this work, we consider processes with identified hadrons in the final state, specifically, single-inclusive electron-positron annihilation (SIA) $e^+e^- \rightarrow hX$, where h denotes the detected hadron and X the remaining, unidentified hadronic remnant. The information of how energetic quarks and gluons that are produced in SIA or other hard-scattering processes subsequently hadronize is encoded in nonperturbative parton-to-hadron fragmentation functions (FFs) [2]. When considering scattering processes involving also hadrons in the initial-state, parton distribution functions (PDFs), the spacelike counterparts of FFs, need to be considered as well.

A reliable quantitative description of inclusive hadron yields within pQCD crucially depends on the precise knowledge of FFs and their uncertainties. In general, these functions are obtained from data through global QCD analyses of certain reference processes [3–8]. Here, SIA data are of utmost importance, similar to the singular role played by deep-inelastic scattering (DIS) measurements in determinations of PDFs. Recently, results from the Belle [9] and BABAR [10] Collaborations have complemented the existing suite of SIA data mainly from the CERN-LEP experiments taken at a center-of-mass system (c.m.s.) energy of $\sqrt{S} = 91.2$ GeV. Thanks to the unprecedented

precision of the new data sets, where the statistical uncertainties are mainly at the subpercent level despite their fine binning, and the lower \sqrt{S} , global QCD analyses can now utilize the energy dependence of the SIA data in the range from about 10.5 to 91.2 GeV [8] to extract FFs also from scaling violations, a key prediction of pQCD.

In order to match the increasing precision of the experimental data sets, the theoretical framework needs to be advanced as well. So far, all global fits of FFs [3–8] were carried out at most at next-to-leading order (NLO) accuracy with still rather sizable theoretical uncertainties due to the truncation of the perturbative series. In this work, we present for the first time an analysis of SIA data at next-to-next-to-leading order (NNLO) in QCD, a level already routinely accomplished in current PDF sets [11] and needed for precision CERN-LHC phenomenology. To reach full NNLO accuracy also for FFs, one first of all needs to include the two-loop coefficient functions for SIA given in Refs. [12–15]. In addition, the FFs exhibit a factorization scale dependence that can be calculated within pQCD and which is governed by a set of coupled equations analogous to the Dokshitzer-Gribov-Lipatov-Altarelli-Parisi evolution equations for PDFs. The required three-loop evolution kernels at $\mathcal{O}(\alpha_s^3)$ in the strong coupling can be found in Ref. [16].

In our phenomenological study of SIA data in terms of FFs, we adopt the technical framework used in the DSS global analyses [6–8] which we extend to NNLO accuracy. As we shall discuss in some detail below, we apply efficient Mellin space techniques in order to both solve the evolution equations and compute the SIA cross section at NNLO. As it turns out, the numerical implementation of the Mellin inverse transformation, needed to compare to data, requires special attention in case of the timelike scale evolution of FFs. We perform global fits to SIA data at leading order

^{*}daniele-paolo.anderle@uni-tuebingen.de[†]marco.stratmann@uni-tuebingen.de[‡]f.ringer@lanl.gov

(LO), NLO, and NNLO accuracy to demonstrate the anticipated reduction in theoretical uncertainties inherent to the truncation of the perturbative calculation at a given fixed order in α_s . We also outline how the quality of the fit gradually improves by including higher-order terms in the global analysis. We note that first reference results for the scale evolution of FFs at $\mathcal{O}(\alpha_s^3)$ were obtained in [17] with which we compare. For the time being, we refrain from including other sources of hadron production data used in the DSS global analyses at NLO accuracy [6–8], hadron multiplicities in semi-inclusive DIS and high transverse momentum hadron production in proton-proton collisions, due to the lack of corresponding NNLO partonic cross sections. As a consequence, our fits will use less free parameters than in the DSS global analyses.

The remainder of the paper is organized as follows: in the next section, we outline all the necessary technical ingredients for the extension of the pQCD framework for SIA to NNLO, specifically, those related to the proper Mellin space implementation and the Mellin inverse transformation. In Sec. III, we briefly recall the DSS global analysis framework and discuss the results of our fits of SIA data up to NNLO accuracy. In particular, we demonstrate the reduction of the scale uncertainty when increasing the perturbative order from LO and NLO to NNLO. In addition, we compare the resulting fragmentation functions to those obtained by DSS [8] and Kretzer [3]. We summarize our main results in Sec. IV, where we also discuss potential further improvements of the presented analysis framework for fragmentation functions.

II. SEMI-INCLUSIVE e^+e^- ANNIHILATION UP TO NNLO ACCURACY

In this section we review the necessary technical aspects to compute SIA cross sections up to NNLO accuracy. Special emphasis is put on the transformation from momentum to Mellin moment space and the additional subtleties appearing beyond NLO. To set the stage, we first recall in Sec. II A the general structure of the SIA cross section. Next, we discuss some relevant features of the NNLO coefficient functions. In Sec. II B we review the timelike evolution equations at NNLO and their truncated and iterated solutions, which we shall compare numerically in Sec. III. Section II C is devoted to a detailed discussion of the numerical implementation of the Mellin space expressions and the proper choice of contour for the Mellin inverse transformation. We will also compare to the results of the MELA evolution code presented in Ref. [17].

A. Cross section and coefficient functions

We consider the SIA process $e^+e^- \rightarrow \gamma/Z \rightarrow hX$ mediated by an intermediate virtual photon γ or Z boson at a c.m.s. energy \sqrt{S} , more specifically, hadron multiplicities defined as

$$\frac{1}{\sigma_{\text{tot}}} \frac{d\sigma^h}{dz} = \frac{1}{\sigma_{\text{tot}}} \left[\frac{d\sigma_T^h}{dz} + \frac{d\sigma_L^h}{dz} \right]. \quad (1)$$

Since we have already integrated over the scattering angle θ of the produced hadron h in (1), parity-violating interference terms vanish, and the cross section $d\sigma^h/dz$ can be decomposed only into a transverse (T) and a longitudinal (L) part, where T, L refer to the γ/Z polarizations [18]. The scaling variable z is defined in terms of the four momenta P_h and q of the observed hadron and γ/Z boson, respectively, as

$$z \equiv \frac{2P_h \cdot q}{Q^2}, \quad (2)$$

where $Q^2 \equiv q^2 = S$, and reduces to the scaled hadron energy $z = 2E_h/\sqrt{S}$ in the e^+e^- c.m.s. frame. Experimental results for Eq. (1) are often given in terms of the scaled hadron three momentum $x_p = 2p_h/\sqrt{S}$, which coincides with z as long as hadron mass effects are negligible.

Up to NNLO accuracy, i.e., $\mathcal{O}(\alpha_s^2)$ in the strong coupling, the total hadronic cross section σ_{tot} in Eq. (1) is given by [13,19]

$$\begin{aligned} \sigma_{\text{tot}} = \sigma_0 N_c \sum_q \hat{e}_q^2 \left[1 + 3C_F a_s + a_s^2 \left(-\frac{3}{2} C_F^2 \right. \right. \\ \left. \left. + C_A C_F \left(-11 \log \left(\frac{Q^2}{\mu_R^2} \right) - 44\zeta(3) + \frac{123}{2} \right) \right. \right. \\ \left. \left. + N_f C_F T_f \left(4 \log \left(\frac{Q^2}{\mu_R^2} \right) + 16\zeta(3) - 22 \right) \right) \right], \quad (3) \end{aligned}$$

where $\sigma_0 = 4\pi\alpha^2/(3Q^2)$ is the lowest order QED cross section for $e^+e^- \rightarrow \mu^+\mu^-$, α denotes the electromagnetic fine structure constant, \hat{e}_q are the electroweak quark charges, and $N_c = 3$ is the number of colors. In addition, we have introduced the usual QCD color factors $C_A = 3$, $C_F = 4/3$, and $T_f = 1/2$. The sum in (3) runs over N_f active massless quark flavors. Here and throughout this paper, we use the definition $a_s = \alpha_s(\mu_R^2)/4\pi$, where μ_R is the renormalization scale. We refrain from reproducing the well-known expressions for the electroweak quark charges which can be found, e.g., in Ref. [13].

The NNLO QCD corrections to the transverse and longitudinal cross sections $d\sigma_k^h/dz$, $k = T, L$, in Eq. (1) were calculated in [12–14]. Adopting the same notation, they can be expressed in factorized form as a convolution of appropriate combinations of quark and gluon fragmentation functions $D_{l=q,g}^h(z, \mu^2)$ and calculable coefficient functions $C_{k,l}^{S,NS}(z, Q^2/\mu^2)$:

$$\begin{aligned} \frac{d\sigma_k^h}{dz} = & \sigma_{\text{tot}}^{(0)} \left[D_S^h(z, \mu^2) \otimes \mathbb{C}_{k,q}^S \left(z, \frac{Q^2}{\mu^2} \right) \right. \\ & \left. + D_g^h(z, \mu^2) \otimes \mathbb{C}_{k,g}^S \left(z, \frac{Q^2}{\mu^2} \right) \right] \\ & + \sum_q \sigma_q^{(0)} D_{\text{NS},q}^h(z, \mu^2) \otimes \mathbb{C}_{k,q}^{\text{NS}} \left(z, \frac{Q^2}{\mu^2} \right), \quad (4) \end{aligned}$$

where, for simplicity, we have set the renormalization scale μ_R equal to the factorization scale μ_F , i.e., $\mu_R = \mu_F \equiv \mu$. The symbol \otimes denotes the standard convolution integral defined as

$$f(z) \otimes g(z) \equiv \int_0^1 dx \int_0^1 dy f(x)g(y)\delta(z - xy). \quad (5)$$

$\sigma_q^{(0)}$ in Eq. (4) is the total quark production cross section for a given flavor q at LO, $\mathcal{O}(\alpha_s^0)$, and $\sigma_{\text{tot}}^{(0)}$ is the corresponding sum over all N_f active flavors. They read $\sigma_q^{(0)} = \sigma_0 N_c \hat{e}_q^2$ and $\sigma_{\text{tot}}^{(0)} = \sum_q \sigma_q^{(0)}$. Factorization in Eq. (4) holds in general only in the presence of a hard scale, in this case Q . Higher-twist corrections to Eq. (4), that are suppressed by inverse powers of the hard scale, can be usually safely neglected as long as Q is large enough. We do not consider them in this study.

The nonperturbative but universal FFs $D_i^h(z, \mu^2)$ have a formal definition as bilocal operators [2] and parametrize the hadronization of a massless (anti)quark or gluon, $i = q, \bar{q}, g$, into the observed hadron h as a function of its fractional momentum z . The fragmentation process is assumed to be independent of any other colored particles produced in a hard scattering. The scale dependence of the FFs is calculable in pQCD and governed by renormalization group equations similar to those for PDFs. The SIA cross section in Eq. (4) depends on the gluon-to-hadron FF $D_g^h(z, \mu^2)$ and the quark singlet (S) and nonsinglet (NS) combinations that are defined as

$$D_S^h(z, \mu^2) = \frac{1}{N_f} \sum_q [D_q^h(z, \mu^2) + D_{\bar{q}}^h(z, \mu^2)] \quad (6)$$

and

$$D_{\text{NS},q}^h(z, \mu^2) = D_q^h(z, \mu^2) + D_{\bar{q}}^h(z, \mu^2) - D_S^h(z, \mu^2) \quad (7)$$

respectively, in terms of the quark plus antiquark FFs $D_q^h(z, \mu^2) + D_{\bar{q}}^h(z, \mu^2)$ for each flavor q .

The corresponding $i = \text{S, NS}$ coefficient functions in Eq. (4) can be calculated perturbatively in pQCD as a series in a_s ,

$$\mathbb{C}_{k,l}^i = \mathbb{C}_{k,l}^{i,(0)} + a_s \mathbb{C}_{k,l}^{i,(1)} + a_s^2 \mathbb{C}_{k,l}^{i,(2)} + \dots, \quad (8)$$

where we have suppressed the arguments $(z, Q^2/\mu^2)$ in (8). Results are available up to $\mathcal{O}(a_s^2)$ [12–14] which is NNLO for the $\mathbb{C}_{T,l}^{\text{S,NS}}$ but formally only of NLO accuracy for the subleading longitudinal coefficient functions $\mathbb{C}_{L,l}^{\text{S,NS}}$. The latter coefficients vanish at $\mathcal{O}(a_s^0)$, and their perturbative series is hence shifted by one power in the strong coupling a_s . The situation is completely analogous to DIS but, unlike in DIS [20], the $\mathcal{O}(a_s^3)$ NNLO contributions have not been calculated yet for SIA. In our phenomenological studies in Sec. III, we will therefore resort, for the time being, to the approximation where the perturbative orders for $\mathbb{C}_{L,l}^{\text{S,NS}}$ are counted as for $\mathbb{C}_{T,l}^{\text{S,NS}}$, i.e., we treat the $\mathcal{O}(a_s^2)$ longitudinal coefficients as NNLO. In that case, the gluon FF does not contribute directly in SIA at LO as also $\mathbb{C}_{T,g}^{i,(0)} = 0$, again, similar to DIS. In addition, we note that up to NLO accuracy, the relation $\mathbb{C}_{k,q}^{\text{S}} = \mathbb{C}_{k,q}^{\text{NS}}$ holds, which can be used to simplify Eq. (4) as was done, e.g., in Ref. [21].

Numerically, in particular, when fitting a large number of data in a global QCD analysis, it is advantageous to work in complex Mellin N moment space rather than with expressions like Eq. (4) containing one or several time-consuming convolution integrals. In general, the Mellin transform $f(N)$ of a function $f(z)$ is defined by

$$f(N) = \int_0^1 dz z^{N-1} f(z). \quad (9)$$

It has the well-known property that convolutions of two functions factorize into ordinary products, i.e., both the transverse and longitudinal cross section $d\sigma_k^h/dz$ in Eq. (4) can be schematically written as products of the Mellin N moments of FFs and coefficient functions, $D_i^h(N, \mu^2) \cdot \mathbb{C}_{k,l}(N, Q^2/\mu^2)$.

The Mellin moments of the NNLO coefficient functions $\mathbb{C}_{k,l}^{i,(2)}$ in (8) were computed in both Refs. [14] and [15]. We analytically checked the consistency of the two results, which are presented using somewhat different notations, by independently calculating the Mellin moments from scratch starting from the z -space expressions given in Appendix C of Ref. [14]. To this end, two MATHEMATICA packages [22,23] were employed. The z -space results in [14] are given in terms of harmonic polylogarithms expressed in the notation H_{m_1, \dots, m_w} , $m_j = 0, \pm 1$ introduced in [24]. Their Mellin transform can be written in terms of harmonic sums

$$S_{a_1, \dots, a_n}(N) = \sum_{k_1=1}^N \sum_{k_2=1}^{k_1} \dots \sum_{k_n=1}^{k_{n-1}} \frac{\text{sign}(a_1)^{k_1}}{k_1^{|a_1|}} \dots \frac{\text{sign}(a_n)^{k_n}}{k_n^{|a_n|}}, \quad (10)$$

where the a_k are positive or negative integers, and N is a positive integer. The number n of a_k indices indicates the so-called depth, whereas $w = \sum_{k=1}^n |a_k|$ is called the

weight of the function. At NNLO accuracy one ends up dealing with harmonic sums of weight up to $w = 4$.

In order to perform the Mellin inverse transformation to z space along a contour in the complex N plane at the very end, see Sec. II C below, one needs to know all functions not only for discrete integers but for any complex value of N . This is achieved by proper analytical continuation of the harmonic sums in Eq. (10). As it is well known [25], there is no analytical continuation for all integer values of N due to the presence of terms $\propto (-1)^N$, and a choice $(-1)^N \rightarrow \pm 1$ has to be made based on physical considerations. For instance, the analytical continuation of all the coefficient functions $C_{k,l}^{\text{S,NS}}$ appearing in Eq. (4) has to correctly reproduce only even integer N moments.

To compare our results for the Mellin moments of the NNLO coefficients obtained with the help of the MATHEMATICA packages [22,23] with those given for even values of N in [14], special care needs to be taken for factors $\propto S_{-2}(N-2)/(N-2)$ since the zero in the denominator for $N = 2$ suggests the presence of a pole. However, this is a spurious pole as can be seen by making use of its the integral representation [26]

$$S_{-2}(N) = - \int_0^1 dz \log(z) \frac{(-z)^N - 1}{1+z}. \quad (11)$$

The existence of this spurious pole for $N = 2$ at NNLO is the reason for the notation adopted in [14], where the Mellin moments of the coefficient functions are written proportional to $\theta(N-3)$ and $\delta(N-2)$, representing the finite $N \rightarrow 2$ limit. Note that the limit in Eq. (11) has to be taken for even N to obtain the correct sign. This can be made manifest by rewriting Eq. (11) in terms of the digamma function which is defined as the derivative of the Euler Gamma function $\psi(x) \equiv d \log[\Gamma(x)]/dx$. The harmonic sum in Eq. (11) then reads [27]

$$S_{-2}(N) = (-1)^{N+3} \beta'(N+1) - \frac{1}{2} \zeta(2), \quad (12)$$

where

$$\beta(N) = \frac{1}{2} \left[\psi\left(\frac{N+1}{2}\right) - \psi\left(\frac{N}{2}\right) \right]. \quad (13)$$

We fully reproduce both the $\theta(N-3)$ pieces and the $N \rightarrow 2$ limits of the NNLO coefficients $C_{k,l}^{\text{S,NS}}(N)$ listed in Ref. [14]. Note that the subtleties concerning the spurious pole for $N = 2$ first appear at the NNLO level. We also completely agree with the results given in Ref. [15] as long as we do not use their definitions of the functions $A_3(N)$, $A_5(N)$, $A_{18}(N)$, $A_{21}(N)$, and $A_{22}(N)$ in Eq. (14) of [15] but, instead, define them as the Mellin transforms of the functions $g_3(x)$, $g_5(x)$, $g_{18}(x)$, $g_{21}(x)$, and $g_{22}(x)$ specified in the ANCONT package [27].

In our numerical code we implement the Mellin N space expressions for the NNLO coefficient functions in the way as they are presented in [15]. The proper analytical continuations of all the harmonic sums and special functions are taken from [15,26–28]. In addition, we are making use of some of the routines provided in the ANCONT package [27].

B. Timelike evolution equations

The factorization procedure invoked in Eq. (4) introduces an arbitrary scale μ_F which conceptually separates the high-energy perturbative regime from the low-energy, nonperturbative region. Both the hard coefficient functions and the FFs depend on μ_F in such a way that at $\mathcal{O}(a_s^n)$ in pQCD any residual dependence of a physical cross section on μ_F is of order $\mathcal{O}(a_s^{n+1})$. Similar to the case of PDFs, this leads to a set of $2N_f + 1$ coupled renormalization group equations (RGEs) governing the scale μ_F dependence of the gluon and N_f quark and antiquark FFs into a given hadron species h . Schematically, these timelike evolution equations read

$$\frac{\partial}{\partial \ln \mu^2} D_i^h(z, \mu^2) = \sum_j P_{ji}^T(z, \mu^2) \otimes D_j^h(z, \mu^2), \quad (14)$$

$i, j = q, \bar{q}, g$, and where, for simplicity, we have set $\mu_R = \mu_F = \mu$ as in Sec. II A. The $j \rightarrow i$ splitting functions $P_{ji}^T(z, \mu^2)$ can be calculated perturbatively as a series in a_s ,

$$P_{ji}^T = a_s P_{ji}^{T,(0)} + a_s^2 P_{ji}^{T,(1)} + a_s^3 P_{ji}^{T,(2)} + \dots, \quad (15)$$

suppressing all arguments z, μ^2 in (15). They are known up to NNLO accuracy [16], i.e., $\mathcal{O}(a_s^3)$, as is the case for their spacelike counterparts P_{ij}^S [29] needed for the scale evolution of PDFs. In fact, there is still a small uncertainty left concerning the off-diagonal splitting kernel $P_{qg}^{T,(2)}$ which could not be completely determined by the crossing relations to the spacelike results employed in [16]. Presumably, this remaining ambiguity is numerically irrelevant for all phenomenological applications; see, however, Ref. [30] for the status of an ongoing direct calculation of the NNLO timelike kernels.

To implement the timelike evolution equations (14) numerically up to NNLO accuracy, we closely follow the strategies and framework developed for the public, spacelike PDF evolution code PEGASUS [31]. In general, the structure and solutions of the spacelike and timelike evolution equations are completely analogous apart from replacing PDFs by FFs and the kernels P_{ij}^S by P_{ji}^T . Hence, for completeness, we repeat here only the most important aspects, in particular, those features appearing for the first time at NNLO.

Instead of working directly with the system of $2N_f + 1$ coupled equations in (14) it is convenient to recast the quark sector into a flavor singlet

$$D_{\Sigma}^h \equiv \sum_q^{N_f} (D_q^h + D_{\bar{q}}^h), \quad (16)$$

which evolves along with the gluon FF D_g^h ,

$$\frac{d}{d \ln \mu^2} \begin{pmatrix} D_{\Sigma}^h \\ D_g^h \end{pmatrix} = \begin{pmatrix} P_{qq}^T & 2N_f P_{gq}^T \\ \frac{1}{2N_f} P_{qg}^T & P_{gg}^T \end{pmatrix} \otimes \begin{pmatrix} D_{\Sigma}^h \\ D_g^h \end{pmatrix}, \quad (17)$$

and $2N_f - 1$ nonsinglet combinations

$$D_{\text{NS},l}^{h,\pm} \equiv \sum_{i=1}^k (D_{q_i}^h \pm D_{\bar{q}_i}^h) - k(D_{q_k}^h \pm D_{\bar{q}_k}^h), \quad (18)$$

$$D_{\text{NS},v}^h \equiv \sum_q^{N_f} (D_q^h - D_{\bar{q}}^h), \quad (19)$$

reflecting the properties of the (anti)quark to (anti)quark splitting functions and which all evolve independently. In Eq. (18) $l = k^2 - 1$, $k = 1, \dots, N_f$, and the subscripts i, k were introduced to distinguish different quark flavors. After the evolution is performed, the individual D_q^h and $D_{\bar{q}}^h$ can be recovered from Eqs. (16), (18), and (19), and any combination relevant for a cross section calculation can be computed, such as those used in the factorized expression for SIA given in Eq. (4).

More specifically, the three NS combinations in Eqs. (18) and (19) evolve with the following NS splitting functions [16]:

$$\begin{aligned} P_{\text{NS}}^{T,\pm} &= P_{qq}^{T,v} \pm P_{q\bar{q}}^{T,v}, \\ P_{\text{NS}}^{T,v} &= P_{\text{NS}}^{T,-} + P_{\text{NS}}^{T,s}, \end{aligned} \quad (20)$$

respectively, and the singlet P_{qq}^T in (17) obeys

$$P_{qq}^T = P_{\text{NS}}^{T,+} + P^{T,ps}. \quad (21)$$

Similarly to the spacelike case, $P_{q\bar{q}}^{T,v} = P_{\text{NS}}^{T,s} = P^{T,ps} = 0$ and $P_{\text{NS}}^{T,s} = 0$ in LO and NLO, respectively, such that three independently evolving NS quark combinations appear for the first time at NNLO accuracy [16]. We note that $P_{\text{NS}}^{T,s} \neq 0$ can lead to a perturbatively generated, albeit small strange-quark asymmetry for FFs, i.e., $D_s^h(z, \mu^2) - D_{\bar{s}}^h(z, \mu^2) \neq 0$, even if the input D_s^h and $D_{\bar{s}}^h$ are symmetric; see Ref. [32] for a detailed discussion of a similar effect in the context of PDFs. For pion FFs such a charge asymmetry is expected to be further suppressed since the effect is driven by a non-zero $D_{\text{NS},v}^h$ in (19). This combination vanishes when exact charge conjugation and isospin symmetry is imposed on the u and d quark and antiquark FFs as is the case in many of the available sets of pion FFs [3–5].

As mentioned already, we choose to solve the set of timelike evolution equations in Mellin N space, which not

only has the benefit of turning all integro-differential equations into ordinary differential equations but also makes them amenable to further analytical studies. Solutions of the evolution equations in N space, as well as their numerical implementation, are well known and were treated extensively in, e.g., Ref. [31] in the spacelike case relevant for PDFs. Since the procedure for FFs is essentially the same, we will in the following only sketch some aspects of the solution at NNLO important for our discussions later on. The needed NNLO kernels $P_{ji}^{T,(2)}(N)$ can be found in [16]. As for the SIA coefficient functions presented in Sec. II A, we have verified the expressions for $P_{ji}^{T,(2)}(N)$ starting from z space and find full agreement.

We start our discussions by recalling the Mellin transformed timelike evolution equations. Adopting the notations used in the PEGASUS code [31], one finds

$$\frac{\partial \mathbf{D}^h(N, a_s)}{\partial a_s} = -\frac{1}{a_s} \left[\mathbf{R}_0(N) + \sum_{k=1}^{\infty} a_s^k \mathbf{R}_k(N) \right] \mathbf{D}^h(N, a_s), \quad (22)$$

where the bold characters indicate that we are dealing in general with 2×2 matrix-valued equations, cf. Eq. (17). For the NS combinations (18) and (19), Eq. (22) reduces to a set of single partial differential equations which are straightforward to solve, and we do not consider them here any further.

The \mathbf{R}_k in (22) are defined recursively as

$$\mathbf{R}_0 \equiv \frac{1}{\beta_0} \mathbf{P}^{T,(0)}, \quad \mathbf{R}_k \equiv \frac{1}{\beta_0} \mathbf{P}^{T,(k)} - \sum_{i=1}^k b_i \mathbf{R}_{k-i}, \quad (23)$$

where $\mathbf{P}^{T,(k)}(N)$ is the k th term in the perturbative expansion of the 2×2 matrix of singlet splitting functions, cf. Eq. (17). In addition, $b_i \equiv \beta_i / \beta_0$ with β_k denoting the expansion coefficients of the QCD β function; see Ref. [33] for explicit expressions up to NNLO, i.e., β_2 . Also note that Eq. (22) is now written in terms of ∂a_s rather than $\partial \log \mu^2$ used in Eq. (14). This convenient change of variables is possible as long as factorization and renormalization scales are related by a constant, i.e., $\mu_R = \kappa \mu_F$, in numerical studies; see Ref. [31] for a detailed discussion. For simplicity, we have so far only considered the case $\mu = \mu_R = \mu_F$. Expressions for $\kappa \neq 1$ can be easily recovered both for the coefficient functions (8) and the splitting functions (15) by reexpanding a_s in powers of $\log(\mu_F^2 / \mu_R^2)$. The general expressions are implemented in our numerical code.

Due to the matrix-valued nature of Eq. (22), no unique closed solution exists beyond LO. Instead, it can be written as an expansion around the LO solution, $(a_s/a_0)^{-\mathbf{R}_0(N)} \mathbf{D}^h(N, a_0)$, where a_0 is the value of a_s at the initial scale μ_0 where the nonperturbative input

$D^h(N, a_0)$ is specified from a fit to data. This expansion reads

$$D^h(N, a_s) = \left[1 + \sum_{k=1}^{\infty} a_s^k U_k(N) \right] \left(\frac{a_s}{a_0} \right)^{-R_0(N)} \times \left[1 + \sum_{k=1}^{\infty} a_s^k U_k(N) \right]^{-1} D^h(N, a_0). \quad (24)$$

The evolution matrices U_k are recursively defined by the commutation relations

$$[U_k, R_0] = R_k + \sum_{i=1}^{k-1} R_{k-1} U_i + k U_k. \quad (25)$$

Based on (24), it is now possible to define several solutions at order N^m LO which are all equivalent up to the accuracy considered, i.e., up to subleading higher-order terms. Any numerical differences between two different choices should be treated as a source of theoretical uncertainty in the determination of FFs or PDFs, and it is expected that the inclusion of NNLO corrections reduces this type of ambiguity as compared to NLO. We highlight two possible solutions which we pursue further in our phenomenological studies in Sec. III. Suppose the perturbatively calculable quantities $P^{T,(k)}$ and β_k are available up to a certain order $k = m$. One possibility is to expand Eq. (24) in a_s and strictly keep only terms up to a_s^m . This defines what is usually called the *truncated solution* in Mellin moment space, and, unless stated otherwise, will be used in all our phenomenological applications.

However, given the iterative definition of the R_k in Eq. (23), one may alternatively calculate the R_k and, hence the U_k in Eq. (25), for any $k > m$ from the known results for $P^{T,(k)}$ and β_k up to $k = m$. Any higher-order $P^{T,(k)}$ and β_k with $k > m$ are simply set to zero. Taking into account all the thus constructed U_k in Eq. (24) defines the so-called *iterated solution*. This solution is important as it mimics the results that would be obtained by solving Eq. (14) directly in z space by some numerical iterative method. Both choices are equally valid as they only differ by terms that are of order $\mathcal{O}(a_s^{m+1})$ and are implemented in our numerical code; see Ref. [31] for a more detailed discussion in the context of spacelike evolution equations. We shall illustrate the numerical differences between the truncated and iterated solution in Sec. III.

C. Numerical implementation

We base the development of our new NNLO evolution code for FFs on the well-tested PEGASUS package [31] which provides different numerical solutions to the spacelike evolution of PDFs up to NNLO accuracy in Mellin N space and the necessary routines for the subsequent Mellin inverse transformation back to momentum space. It also

solves the RGE for the strong coupling $a_s(\mu_R^2)$ in the required order in pQCD. In addition to extending PEGASUS to handle also timelike evolution, we also add packages to compute the SIA cross section in N space and to determine the parameters of the FFs at some input scale μ_0 from a fit to existing SIA data at LO, NLO, and NNLO accuracy.

In Sec. II B we have omitted how we deal with heavy quark flavors, i.e., charm and bottom, in the timelike scale evolution apart from defining the relevant $2N_f - 1$ NS combinations of FFs in Eqs. (18) and (19). In PEGASUS [31] both a fixed flavor-number scheme (FFNS) and a variable flavor-number scheme (VFNS) evolution are implemented. For the latter, matching coefficients between the spacelike evolution for N_f and $N_f + 1$ are provided for both PDFs [34] and the RGE for a_s [35] up to NNLO accuracy. Similar timelike matching coefficients for FFs are only known up to NLO and can be found in Ref. [36]. They are implemented in our evolution code. In practice, however, all fits of FFs performed so far [3–8], have used a different approach for the charm and bottom-to-light hadron FFs. Once the scale μ in the evolution crosses the heavy quark pole mass $Q = m_{c,b}$, a new nonperturbative input distribution is introduced at that scale $D_{c,b}^h(z, m_{c,b}^2)$ and $N_f \rightarrow N_f + 1$. The parameters describing these input distributions $D_{c,b}^h(z, m_{c,b}^2)$ are also determined by a fit to, usually flavor-tagged, data taken at scales $\mu \gg m_{c,b}$. We will also adopt this nonperturbative input scheme (NPIS) in all our phenomenological studies below. We note that as one of the many cross-checks for our new timelike evolution code, we have implemented the input parameters and $a_s(\mu_0)$ value of the NLO NPIS fit to SIA data performed in Ref. [3]. We obtain an excellent numerical agreement with the FFs of [3] for all z and μ values.

As the last technical issue, we would like to comment on the numerical implementation of the Mellin inverse transformation. To this end, one needs to perform a numerical integration in complex N space along a suitably chosen contour \mathcal{C}_N in order to recover expressions in z space which can be compared to data. In case of the SIA cross section, this transformation schematically reads

$$D(z) \otimes \mathbb{C}(z) = \frac{1}{2\pi i} \int_{\mathcal{C}_N} dN z^{-N} D(N) \mathbb{C}(N), \quad (26)$$

where we have omitted any scale μ and flavor dependence in Eq. (26). In practice, one chooses a tilted contour \mathcal{C}_N which can be parametrized in terms of a real variable x as $N = c + x e^{i\phi}$; see Fig. 1 for an illustration of the path and Ref. [31] for more details. To ensure that the value of the integral is independent of \mathcal{C}_N , c has to be to the right of the rightmost pole of the integrand, which, in our case, are all located along the real axis. An exponential dampening of the integrand in (26) is achieved for $\pi > \phi \geq \pi/2$, resulting in a smaller upper integration limit x_{\max} sufficient for a numerically stable result.

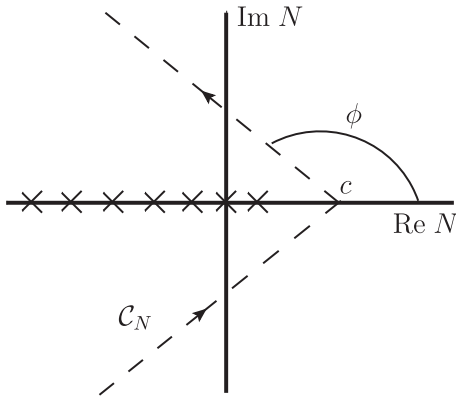


FIG. 1. The dashed line represents the contour \mathcal{C}_N in complex N space to perform the inverse Mellin transformation (26). The poles of the integrand along the real axis are schematically represented by the crosses.

However, extra care needs to be taken in choosing actual values for both c and ϕ beyond the requirements just outlined. As it turns out, the standard choice, $c = 1.9$ and $\phi = 3/4$, made for the PDF evolution in PEGASUS cannot be used in the timelike case. This is due to the fact that the timelike kernels $P^T(z)$ are more singular than their spacelike counterparts $P^S(x)$ in the limit $z, x \rightarrow 0$. At NLO accuracy, one finds, for instance, that $P_{gg}^{T,(1)}(z) \propto \log^2(z)/z$ [16] whereas $P_{gg}^{S,(1)}(x) \propto 1/z$ [29]. In Mellin space this behavior translates into $\propto 1/(N-1)^3$ and $\propto 1/(N-1)$, respectively, i.e., a leading singularity at $N = 1$. To order N^{mLO} this generalizes to $P_{gg}^{T,(m)}(N) \propto 1/(N-1)^{(2m+1)}$ [37] whereas in the spacelike case only one additional power of $1/(N-1)$ appears in each order [38]. As a result, the function that is integrated in Eq. (26) has potentially much stronger oscillations in the vicinity of the pole $N = 1$ than for the corresponding Mellin inverse transformations for spacelike PDFs and observables, and achieving numerical convergence becomes considerably more delicate.

To illustrate this issue further, we schematically write the general solution in Eq. (24) as

$$\mathbf{D}^h(N, a_s) = \begin{pmatrix} \mathcal{K}_{11}^T(a_s, a_0, N) & \mathcal{K}_{12}^T(a_s, a_0, N) \\ \mathcal{K}_{21}^T(a_s, a_0, N) & \mathcal{K}_{22}^T(a_s, a_0, N) \end{pmatrix} \mathbf{D}^h(N, a_0), \quad (27)$$

where the \mathcal{K}_{ij}^T denote the entries of the 2×2 timelike evolution matrix on the right-hand side of (24). A similar equation can be written down for the evolution of PDFs.

In Fig. 2 we show a comparison of the real part of the NLO singlet evolution kernel $\text{Re}\{\mathcal{K}_{12}^{T,S}\}$ for the truncated solution for both the evolution of FFs (upper panel) and PDFs (lower panel) in the relevant section of the complex N plane. As an illustrative example, we have chosen $\mu_0^2 = 1 \text{ GeV}^2$ and $\mu^2 = 110 \text{ GeV}^2$, the scale relevant for Belle

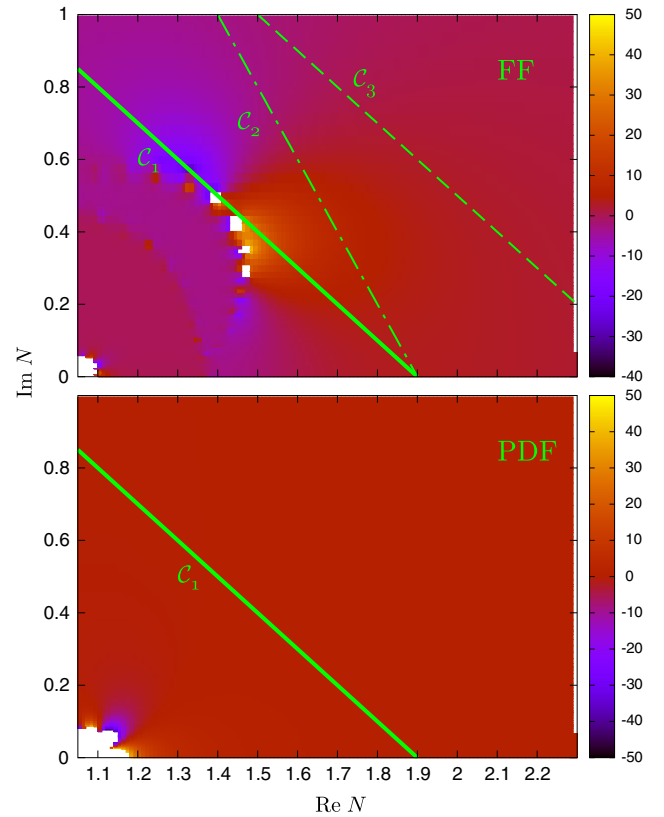


FIG. 2 (color online). The value of the real part of \mathcal{K}_{12}^T in Eq. (27) in a region of the complex N plane for both the evolution of FFs (upper panel) and PDFs (lower panel). The lines correspond to three different integration contours \mathcal{C}_N in (26). \mathcal{C}_1 is the default choice in the PEGASUS package [31]; see text.

and BABAR, in Eq. (27). The line labeled as \mathcal{C}_1 represents the standard contour \mathcal{C}_N implemented in PEGASUS [31], and $\mathcal{C}_{2,3}$ are two alternative choices.

As can be seen from the upper panel of Fig. 2, the contour \mathcal{C}_1 with $c = 1.9$ and $\phi = 3/4$ goes through a region of strong numerical oscillations of $\text{Re}\{\mathcal{K}_{12}^T\}$ and, as a consequence, yields numerically unstable results for the integral in Eq. (26). Hence, in our code we need to choose either a different angle, e.g., $\phi = 2/3$ as in \mathcal{C}_2 , or a different value of c , such as $c = 2.5$ adopted in \mathcal{C}_3 . Both choices lead to numerically stable and identical results for the Mellin inverse transformation in Eq. (26) for all practical purposes. Figure 2 also shows that no such issue appears for the evolution of PDFs because of the weaker $N = 1$ singularity than in the timelike case.

Finally, we compare the results of our timelike evolution code with those obtained with the publicly available MELA [17] package, where also tables of benchmark numbers are given corresponding to input FFs taken from the fit in Ref. [5]; cf. Eq. (3.3) in [17]. Using the same input FFs, we were not able to directly reproduce their benchmark results as generated “out of the box” from the downloadable script. The RGE for $a_s(\mu_R)$ is always solved exactly in our code by

means of a fourth order Runge-Kutta integration [39] (as taken from the PEGASUS package [31]), whereas in MELA the standard, expanded solution is utilized for the truncated solution of Eq. (24). After this small difference is accounted for, we achieve perfect numerical agreement with differences of less than 0.01% for both the truncated and iterated solution using the FFNS with $N_f = 3$ or the VFNS.

III. PHENOMENOLOGICAL APPLICATIONS

As a first application of our timelike evolution package presented in Sec. II, we will perform a fit to the available SIA data with identified pions up to NNLO accuracy in Sec. III A. The obtained sets of LO, NLO, and NNLO pion FFs will be used in Sec. III B to demonstrate the relevance of the NNLO corrections to the SIA cross section and to estimate the residual theoretical uncertainties due to variations of the factorization scale in each order or to the choice of a truncated or iterated variant of the solution to the evolution equations given in (24).

A. Fit of pion FFs up to NNLO accuracy

Since full NNLO corrections are only available for a rather limited set of hard-scattering processes, we have to restrict our first analysis of FFs at NNLO accuracy to data obtained in SIA for the time being. In addition, we focus solely on pion production where data are most abundant and precise. In any case, the main interest of this work are the general features of NNLO corrections rather than to provide a new set of FFs.

To facilitate the fitting procedure, we closely follow the framework outlined and used in the series of DSS global QCD analyses of parton-to-pion FFs at NLO accuracy [6–8]. Specifically, we adopt the same flexible functional form

$$D_i^{\pi^+}(z, \mu_0^2) = \frac{N_i z^{\alpha_i} (1-z)^{\beta_i} [1 + \gamma_i (1-z)^{\delta_i}]}{B[2 + \alpha_i, \beta_i + 1] + \gamma_i B[2 + \alpha_i, \beta_i + \delta_i + 1]} \quad (28)$$

to parametrize the nonperturbative input FFs for charged pions at a scale μ_0 in the $\overline{\text{MS}}$ scheme. Here, $B[a, b]$ is the Euler Beta function used to normalize the parameter N_i in (28) for each flavor i to its contribution to the energy-momentum sum rule. In addition to the gluon $i = g$, we only consider FFs for the sum of a quark and an antiquark of a given flavor i , i.e., $i = u + \bar{u}$, $d + \bar{d}$, $s + \bar{s}$, $c + \bar{c}$, and $b + \bar{b}$, since SIA is only sensitive to $q + \bar{q}$ flavor combinations as can be already inferred from Eq. (4). Also, since all hadrons in SIA originate from the initially produced $q\bar{q}$ pair, the rates for π^+ and π^- are the same, and data for charged pions are usually presented for the sum $d\sigma^\pi \equiv d\sigma^{\pi^+} + d\sigma^{\pi^-}$.

We assume charge conjugation and isospin symmetry and impose $D_{u+\bar{u}}^{\pi^+} = D_{d+\bar{d}}^{\pi^+}$ as is also suggested by the flavor

composition of π^\pm . We note that a recent global QCD analysis of pion FFs at NLO accuracy based on SIA, SIDIS, and pp data [8] finds a breaking of this symmetry of less than 0.5%. Beyond that, we are forced to fix certain parameters in our *ansatz* (28) as they cannot be constrained by data. More specifically, we set $\alpha_{s+\bar{s}} = \alpha_{u+\bar{u}}$, $\beta_{s+\bar{s}} = \beta_{u+\bar{u}} + \delta_{u+\bar{u}}$, and $\beta_g = 8$. In addition, $\delta_{g,s+\bar{s},c+\bar{c}} = 0$ and $\gamma_{g,s+\bar{s},c+\bar{c}} = 0$. For light quark flavors and the gluon, we choose an initial scale of $\mu_0 = 1$ GeV. As in all previous fits [3–8], the charm and bottom-to-pion FFs are treated as a nonperturbative input and are turned on discontinuously at $\mu_0^c = m_c = 1.4$ GeV and $\mu_0^b = m_b = 4.75$ GeV, respectively. Their parameters are essentially determined by charm and bottom flavor-tagged SIA data. In case of $D_{b+\bar{b}}^{\pi^+}$, a good fit is only achieved with the full functional form (28) using all five parameters, whereas for charm only three free parameters are needed. Since the heavy quark masses are neglected throughout in the NPIS, $D_{c+\bar{c}}^{\pi^+}$ and $D_{b+\bar{b}}^{\pi^+}$ should be only used in cross sections such as Eq. (4) at scales well beyond their partonic thresholds $\mu = 2m_c$ and $\mu = 2m_b$, respectively.

The remaining 16 free parameters are determined by a standard χ^2 minimization procedure as described, for instance, in Ref. [8]. They are listed in Table I for our LO, NLO, and NNLO sets of pion FFs. For each set of experimental data we determine the optimum normalization shift analytically and assign an additional contribution to χ^2 according to the quoted experimental uncertainties; see, e.g., Eq. (5) in Ref. [8] for details.

Our fits are performed to the following sets of inclusive and flavor-tagged SIA data with identified pions: SLD [40], Aleph [41], Delphi [42], and Opal [43], all taken at a c.m.s. energy of $\sqrt{S} = 91.2$ GeV, TPC [44] at $\sqrt{S} = 29$ GeV, and BABAR [10] and Belle [9] both at $\sqrt{S} = 10.5$ GeV. The SLD, Delphi and TPC experiments not only provide inclusive SIA measurements but also uds , charm and bottom-tagged data. All these sets were also used in the recent global analysis presented in Ref. [8].

As is customary [3–8], we do not include any data below a certain z_{\min} in the fit where finite, but neglected hadron mass effects $\propto M_\pi/(z^2 S)$ might become relevant [45], and potentially large logarithmic contributions $\propto \log z$, briefly mentioned in Sec. II C, need to be resummed to all orders [37,46,47]. For all our fits, we choose $z_{\min} = 0.075$. In addition, we employ an upper cut of $z < z_{\max} = 0.95$. In this region threshold logarithms $\propto \log(1-z)$ in the coefficient functions are expected to become increasingly relevant, and, again, all-order resummations are needed [45,48]. Resummations are rather straightforward to implement in Mellin N space, and, hence, we plan to extend our code further by including them based on the knowledge that can be gathered from all the available fixed order results at

TABLE I. Parameters describing our optimum LO, NLO, and NNLO $D_i^{\pi^+}(z, \mu_0)$ in Eq. (28) at the input scale $\mu_0 = 1$ GeV. Results for the charm and bottom FFs refer to the scales $\mu_0^c = m_c = 1.4$ GeV and $\mu_0^b = m_b = 4.75$ GeV, respectively. The parameters given in italics are fixed by $\alpha_{s+\bar{s}} = \alpha_{u+\bar{u}}$, $\beta_{s+\bar{s}} = \beta_{u+\bar{u}} + \delta_{u+\bar{u}}$, and $\beta_g = 8$ but are listed for completeness.

Parameter	LO	NLO	NNLO
$N_{u+\bar{u}}$	0.735	0.572	0.579
$\alpha_{u+\bar{u}}$	-0.371	-0.705	-0.913
$\beta_{u+\bar{u}}$	0.953	0.816	0.865
$\gamma_{u+\bar{u}}$	8.123	5.553	4.062
$\delta_{u+\bar{u}}$	3.854	1.968	1.775
$N_{s+\bar{s}}$	0.243	0.135	0.271
$\alpha_{s+\bar{s}}$	<i>-0.371</i>	<i>-0.705</i>	<i>-0.913</i>
$\beta_{s+\bar{s}}$	<i>4.807</i>	<i>2.784</i>	<i>2.640</i>
N_g	0.273	0.211	0.174
α_g	2.414	2.210	1.595
β_g	<i>8.000</i>	<i>8.000</i>	<i>8.000</i>
$N_{c+\bar{c}}$	0.405	0.302	0.338
$\alpha_{c+\bar{c}}$	-0.164	-0.026	-0.233
$\beta_{c+\bar{c}}$	5.114	6.862	6.564
$N_{b+\bar{b}}$	0.462	0.405	0.445
$\alpha_{b+\bar{b}}$	-0.090	-0.411	-0.695
$\beta_{b+\bar{b}}$	4.301	4.039	3.681
$\gamma_{b+\bar{b}}$	24.85	15.80	11.22
$\delta_{b+\bar{b}}$	12.25	11.27	9.908

NNLO accuracy for both $z \rightarrow 0$ and $z \rightarrow 1$ in a dedicated future work.

We note that we are not fitting the initial value a_s at some reference scale in order to solve the RGE governing the running of the strong coupling but rather adopt the following boundary conditions $\alpha_s(M_Z) = 0.135$ at LO, $\alpha_s(M_Z) = 0.120$ at NLO, and $\alpha_s(M_Z) = 0.118$ at NNLO accuracy from the recent MMHT global analysis of PDFs; see the first reference in [11].

Table II and Fig. 3 illustrate the quality of our fits to SIA data at LO, NLO, and NNLO accuracy in terms of the individual χ^2 values obtained for each experiment and the quantity “[data-theory]/theory,” respectively. The total χ^2 penalty originating from the normalization shifts applied to each data set can be also found at the bottom of Table II. It turns out to be small, about 7 units, and is largely independent of the perturbative order. Upon applying the cuts on the z range discussed above, a total of 288 data points remains for the fitting procedure and to determine the 16 free parameters describing our parton-to-pion FFs $D_i^{\pi^+}(z, \mu_0)$ in Eq. (28). All fits yield a very good χ^2 per degree of freedom (d.o.f.) ranging from 0.89 in LO to 0.64 at NNLO accuracy. We note, however, that the $\chi^2/\text{d.o.f.}$ would deteriorate very significantly if the number of free fit parameters would be reduced further by setting, for instance, $\gamma_{u+\bar{u}} = 0$ or $\gamma_{b+\bar{b}} = 0$.

TABLE II. The individual χ^2 values and number of points for each inclusive and flavor-tagged data set included in our fits at LO, NLO, and NNLO accuracy. At the bottom, we list the total χ^2 penalty from the normalization shifts and the total χ^2 for each fit.

Experiment	Data type	# data in fit	χ^2			
			LO	NLO	NNLO	
SLD [40]	Inclusive	23	15.0	14.8	15.5	
	<i>uds tag</i>	14	9.7	18.7	18.8	
	<i>c tag</i>	14	10.4	21.0	20.4	
Aleph [41]	<i>b tag</i>	14	5.9	7.1	8.4	
	Inclusive	17	19.2	12.8	12.6	
	Inclusive	15	7.4	9.0	9.9	
Delphi [42]	<i>uds tag</i>	15	8.3	3.8	4.3	
	<i>b tag</i>	15	8.5	4.5	4.0	
	Inclusive	13	8.9	4.9	4.8	
Opal [43]	Inclusive	13	5.3	6.0	6.9	
TPC [44]	<i>uds tag</i>	6	1.9	2.1	1.7	
	<i>c tag</i>	6	4.0	4.5	4.1	
	<i>b tag</i>	6	8.6	8.8	8.6	
BABAR [10]	Inclusive	41	108.7	54.3	37.1	
Belle [9]	Inclusive	76	11.8	10.9	11.0	
Normalization shifts			7.4	6.8	7.1	
TOTAL:			288	241.0	190.0	175.2

As can be seen from Table II and Fig. 3, nearly all SIA data sets can be described equally well in LO, NLO, and NNLO accuracy with just a few exceptions, most notably the *BABAR* data [10] taken at the smallest \sqrt{s} which drive the differences found in the total χ^2 values of the three fits. Here, the inclusion of higher-order corrections progressively leads to better fits. A closer inspection reveals that the larger χ^2 at LO, and also at NLO, stems from the data points corresponding to the lowest z values included in the fit, i.e., $0.075 \leq z \lesssim 0.12$; note that the Belle Collaboration does not provide any data below $z = 0.2$. This result is readily understood from the fact that calculations at higher orders contain more of the numerically important small z enhancements $\propto \log z$ mentioned above, i.e., are closer to an all-order result. From the observation that calculations at NNLO accuracy provide a significantly better description of data at small z , one can anticipate that including all-order resummations into the analysis framework would eventually further extend the range of z amenable to pQCD. We will investigate this quantitatively in a future publication. The neglected hadron mass is another source of potentially large corrections at small z and/or \sqrt{s} . In Ref. [45] it was shown, however, that hadron mass terms are relatively small for pion production in SIA in the kinematic regime relevant for the *BABAR* data. We also wish to recall that *BABAR* provides their data in two variants called “conventional” and “prompt,” differing by the treatment of weak decays into pions in their event sample [10]. As in the recent global NLO analysis [8], our results are based on the latter set. We have verified that a decent fit to all SIA data

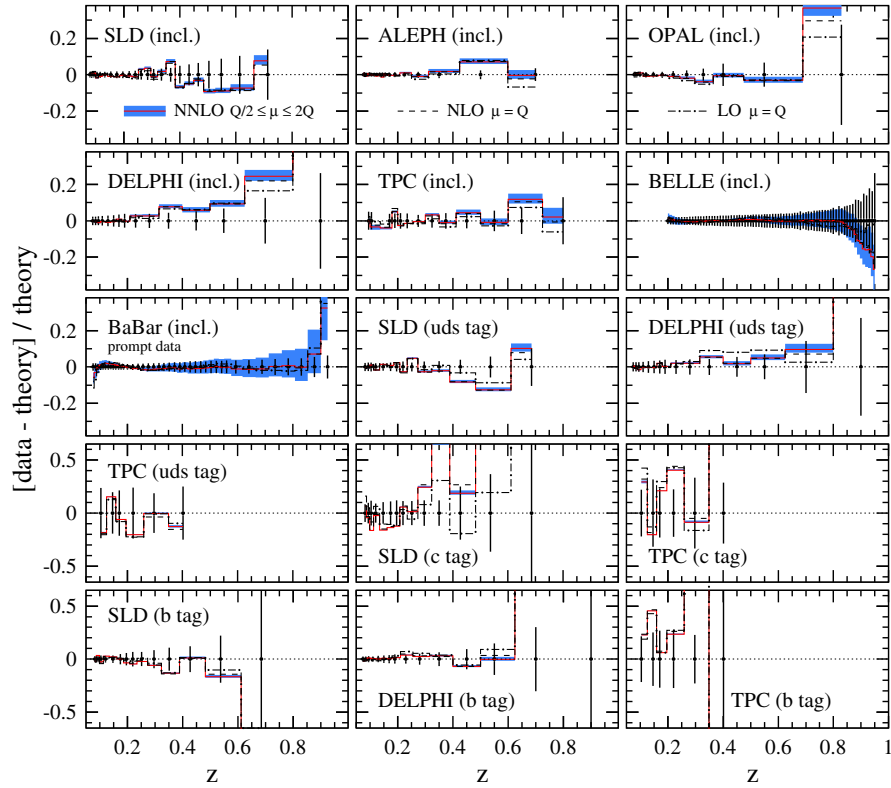


FIG. 3 (color online). Ratios for $[\text{data} - \text{theory}] / \text{theory}$ for our LO (dot-dashed), NLO (dashed), and NNLO (solid lines) fits computed with the scale $\mu = Q$ for the data sets listed in Table II. The shaded bands illustrate the remaining scale ambiguity at NNLO accuracy in the range $Q/2 \leq \mu \leq 2Q$. The points along the zero axis indicate the relative experimental uncertainty.

can be also obtained when the “conventional” data are used instead but at the expense of a less favorable total χ^2 , e.g., 236.4 rather than 190.0 units at NLO, and, more importantly, for undesirable corners of the parameter space describing the $D_i^{\pi^+}(z, \mu_0)$ in Eq. (28). For instance, the $u + \bar{u}$ fragmentation tends to saturate the energy-momentum sum rule, which is summed over all hadrons, already for pions.

Table II and Fig. 3 also reveal that some flavor-tagged data from SLD can be described best at LO but at the expense of larger χ^2 values for inclusive Aleph and Opal data. In general, the NLO and NNLO results are very similar for all data sets used in the fits except, as just discussed, for a few points from *BABAR* at small z . This observation also carries over to the obtained FFs at NLO and NNLO accuracy, in particular, those flavor combinations which are constrained best by the SIA data alone.

Figure 4 shows our fitted LO, NLO, and NNLO $D_i^{\pi^+}(z, Q^2)$ at $Q^2 = 10 \text{ GeV}^2$ for $i = u + \bar{u}$, $s + \bar{s}$, g , and the flavor singlet combination in (16) for $N_f = 4$. As a comparison with previous NLO results, we consider the most recent global analysis of the DSS group [8], based on the same set of SIA data plus SIDIS and pp data, and the old fit by Kretzer [3]. The latter still provides a good description of all pion data, including those from SIDIS and

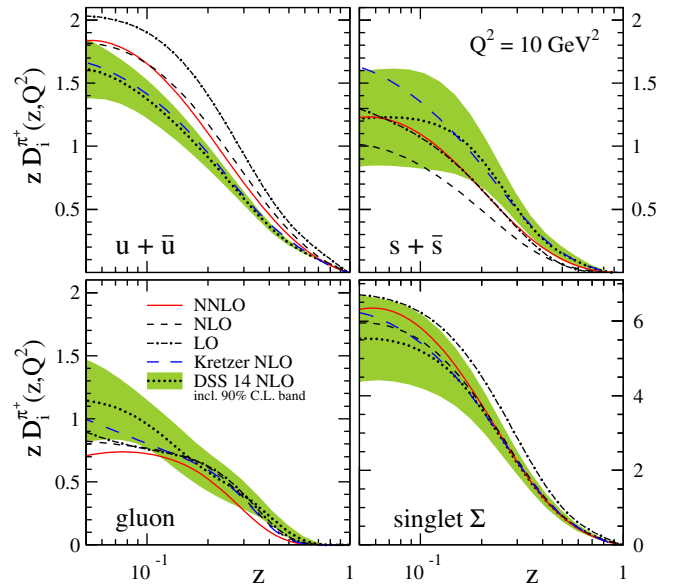


FIG. 4 (color online). Comparison of our LO, NLO, and NNLO FFs $D_i^{\pi^+}(z, Q^2)$ at $Q^2 = 10 \text{ GeV}^2$ for $i = u + \bar{u}$, $s + \bar{s}$, g , and the flavor singlet combination in (16) for $N_f = 4$. Also shown are the optimum NLO FFs from Kretzer [3], obtained also solely from SIA data, and the latest global analysis of the DSS group [8] based on SIA, SIDIS, and pp data. For the latter, we also illustrate their 90% C.L. uncertainty estimates (shaded bands).

pp , despite making use of only a small subset of the SIA data listed in Table II comprising SLD [40], Aleph [41], and TPC [44]. To illustrate how the current experimental uncertainties typically propagate to the extraction of parton-to-pion FFs, we also show in Fig. 4 the 90% confidence level (C.L.) estimates of the latest DSS global QCD fit (shaded bands). As was already mentioned, we refrain from providing uncertainty bands for our fits as SIA data alone are not sufficient for providing a reliable estimate due to the assumptions one has to impose on the parameter space describing the $D_i^{\pi^+}(z, \mu_0)$ in Eq. (28).

From Fig. 4 one can make the following observations: the quantity which is known to be constrained best by the SIA data alone [3–8], the flavor singlet combination $D_{\Sigma}^{\pi^+}$ defined in Eq. (16), is very similar for all the NLO results, DSS, Kretzer, and our fit, in particular, for $z \gtrsim 0.1$. The fact that also the singlet FF determined at NNLO accuracy is close to the NLO results gives some indication that NNLO corrections do not seem to alter results obtained at NLO accuracy too much. A similar level of agreement for $D_{\Sigma}^{\pi^+}$ is found also at other scales, for instance, $\mu = M_Z$.

Breaking up the singlet into FFs for individual quark flavors depends on the assumptions made in the fit, including such details as the choice for z_{\min} . Therefore, it is not too surprising that one finds some differences between the various fits shown in Fig. 4 for the favored $D_{u+\bar{u}}^{\pi^+}$ and the unfavored $D_{s+\bar{s}}^{\pi^+}$, with the latter FF, of course, being considerably less well constrained by data than the former. Another FF which is only loosely constrained by a fit to solely SIA data is the gluon $D_g^{\pi^+}$, which, despite the different assumptions, agrees rather well among all fits. Finally, one notices that for a LO fit both the singlet and the favored FFs, $D_{\Sigma}^{\pi^+}$ and $D_{u+\bar{u}}^{\pi^+}$, respectively, are significantly larger than the corresponding NLO estimates. In general, we find that in order to achieve a good fit to SIA data at LO accuracy, some of the parameters listed in Table I tend to approach extreme values, for instance, the $u + \bar{u}$ fragmentation saturates most of the energy-momentum sum rule already for pions. In any case, LO estimates are not sufficient for phenomenological applications.

B. Impact of NNLO corrections on theoretical uncertainties

In this section we analyze the relevance of the NNLO corrections for a reliable phenomenology of the SIA process. To this end, we will examine the importance of various sources of theoretical uncertainties in LO, NLO, and NNLO accuracy. We will present results for the size of the NNLO corrections in terms of the K factor, study the residual dependence on the choice of scale μ , and investigate the uncertainties induced by choosing a particular solution, truncated or iterated, to the timelike evolution equations. All these results are largely independent of the

details of fitting an actual set of FFs, and as such they represent the main numerical results of this paper along with our newly developed NNLO code described in Sec. II.

In Fig. 5, we show the K factor for the SIA process defined as $d\sigma^{\pi}(\text{N}^m\text{LO})/d\sigma^{\pi}(\text{N}^{m-1}\text{LO})$ for $m = 2$ (solid) and $m = 1$ (dashed lines) for the three c.m.s. energies corresponding to the experiments included in our fit; see Table II. To determine only the impact of the genuine higher-order corrections and not some numerical differences in the LO, NLO, and NNLO FFs, like those illustrated in Fig. 4, all calculations in Fig. 5 are performed with our NLO input FFs. Their evolution, the running of the strong coupling a_s , and the coefficient functions are taken consistently either at LO, NLO, or NNLO accuracy though.

As one expects, the K factor for the NNLO/NLO results is significantly smaller than the one for NLO/LO, and for most values of z the additional NNLO corrections are at the level of about 10% or less. Both at large and small z , one finds clear indications for the presence of large logarithmic corrections to the perturbative series contained in the evolution kernels P^T and the SIA coefficient functions \mathbb{C} . They need to be resummed to all orders to extend the range of applicability of the presented fixed order results to both $z \rightarrow 1$ and $z \rightarrow 0$. We note that the small \sqrt{S} dependence of the K factors in Fig. 5 is only caused by the different orders in pQCD used in the denominator and

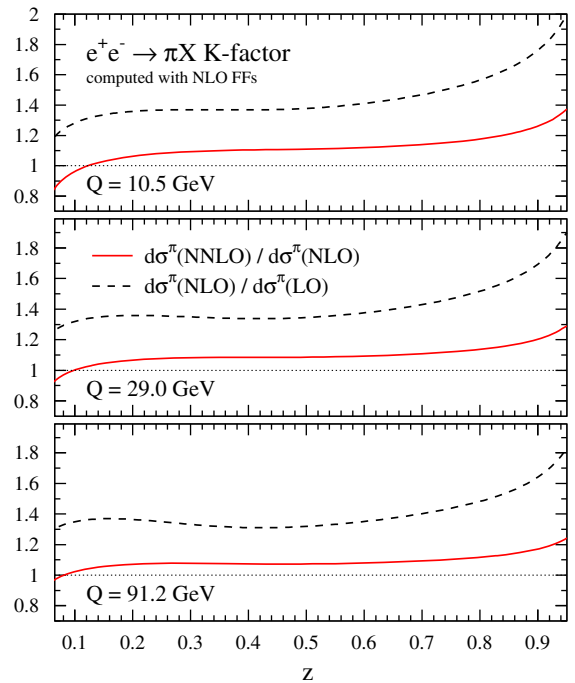


FIG. 5 (color online). NNLO/NLO (solid) and NLO/LO (dashed lines) K factors for the SIA process for three different c.m.s. energies. All computations are performed with our NLO set of parton-to-pion FFs; see text.

in the numerator, $d\sigma^\pi(N^m\text{LO})$ and $d\sigma^\pi(N^{m-1}\text{LO})$, respectively, to compute the scale evolution of FFs and the coupling a_s . There is no scale in the coefficient functions as we have set $\mu_R = \mu_F = \mu = Q$ throughout, i.e., all logarithms of the type $\log(\mu_R^2/\mu_F^2)$ or $\log(Q^2/\mu_F^2)$ vanish.

The scale dependence of the SIA cross section is illustrated in Fig. 6, where we show results at LO, NLO, and NNLO accuracy (shaded bands) for $\mu_R = \mu_F = \mu = 2Q$ and $\mu = Q/2$ normalized in each case to our default choice $\mu = Q$. The residual dependence on the choice of the scale μ in a theoretical calculation is presumably the most important source of uncertainty and is expected to shrink progressively upon including higher and higher-order corrections. This is exactly what we find. For instance, at $\sqrt{S} = 10.5$ GeV, relevant for *BABAR* and *Belle*, the typical scale uncertainty at $z \approx 0.5$ amounts to about 20% at LO and reduces to $\approx 10\%$ at NLO and $\approx 5\%$ at NNLO. At larger c.m.s. energies, the scale ambiguities are even smaller and reach around 1%–2% at NNLO accuracy. This is actually needed in a phenomenological analysis to roughly match the experimental uncertainties for the most precise sets of inclusive pion data as can be inferred from Fig. 3; note that the scale uncertainty bands are hardly visible for some of the flavor-tagged data as we had to inflate the axis of the ordinate in Fig. 3 to accommodate the rather sizable experimental uncertainties.

As can be seen from Fig. 6, all scale uncertainty bands narrow down somewhere in the range $0.1 \lesssim z \lesssim 0.15$

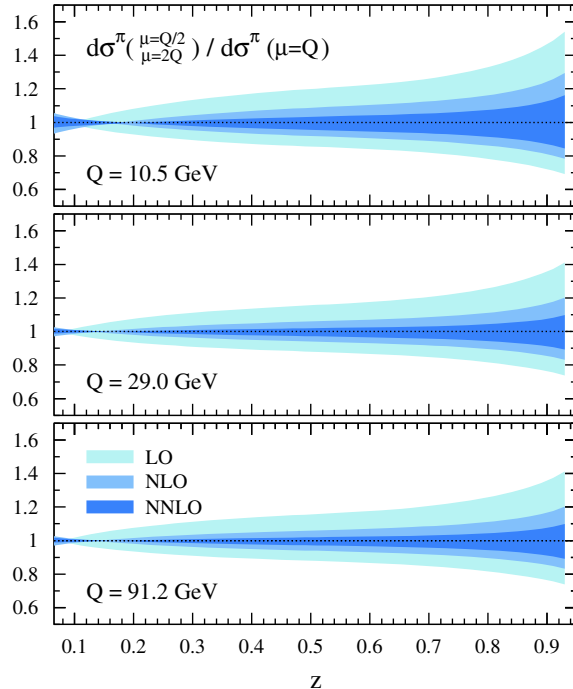


FIG. 6 (color online). Scale dependence of the SIA cross section at LO, NLO, and NNLO accuracy in the range $Q/2 \leq \mu = \mu_R = \mu_F \leq 2Q$ normalized to the results obtained for $\mu = Q$ for three values of \sqrt{S} .

before they start to increase again towards $z \rightarrow 0$. This can be readily understood from fact that one has approximate “scaling” of the SIA cross section, or, alternatively, the quark FFs, for some value of z in this region, i.e., they become independent of the scale μ . This is very much similar to DIS and PDFs, where this happens somewhere near momentum fractions of about 0.2. Of course, QCD corrections always introduce some scale dependence, and higher-order cross sections never probe a FFs or a PDFs locally at one value of momentum fraction but rather over a broad range due to the presence of convolutions, like, for instance, in Eq. (4).

We close our discussions about the relevance of the NNLO corrections by showing the theoretical ambiguity associated with the different choices one has in defining the solution to the timelike evolution equations beyond the LO accuracy. More specifically, Fig. 7 gives the ratio of the iterated and truncated variant of the general solution given in Eq. (24) computed in NLO (dashed) and NNLO (solid line); see also the corresponding discussions in Sec. II B. In the z range relevant for the extraction of FFs from data, this type of theoretical uncertainty is rather small, and we note that it is usually not considered or even mentioned [3–8]. As for the K factor and the scale dependence shown in Figs. 5 and 6, respectively, including NNLO corrections reduces the residual uncertainties by about a factor of 2 as compared to the results obtained at NLO accuracy. For most values of z , the differences between the truncated and iterated solutions are less than 0.5% at NNLO, i.e., smaller than scale uncertainties and potentially missing higher-order corrections as indicated by the K factor for NNLO/NLO.

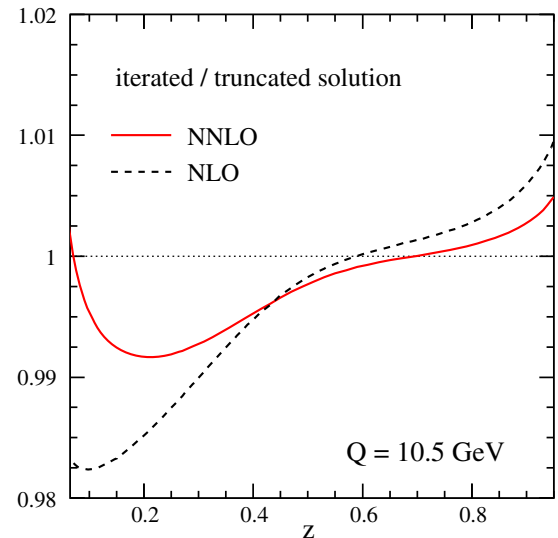


FIG. 7 (color online). Ratio of the iterated and truncated variant of the solution (24) to the timelike evolution equations at NLO (dashed) and NNLO (solid line) accuracy at the scale of the *BABAR* and *Belle* experiments.

IV. CONCLUSIONS AND OUTLOOK

We have presented a first analysis of parton-to-pion fragmentation functions at next-to-next-to-leading order accuracy in QCD based on single-inclusive pion production in electron-positron annihilation. To this end, we have extended the existing spacelike evolution package PEGASUS for parton distribution functions to the timelike region and fragmentation functions. The code is numerically very efficient and works throughout in Mellin N moment space, where the evolution equations can be solved analytically.

We have discussed all the relevant technical details to perform the QCD scale evolution and cross section calculation for single-inclusive hadron production in electron-positron annihilation up to next-to-next-to-leading order accuracy. We have verified all the needed expressions for the N moments of the timelike evolution kernels and the hard-scattering coefficient functions by rederiving them from their counterparts in momentum space. We find full agreement with the results given in the literature. The results obtained with our timelike evolution code are found to agree with the MELA package after correcting some obvious inconsistency in generating their benchmark numbers.

On the phenomenological side, we have extracted new sets of parton-to-pion fragmentation functions from a fit to electron-positron annihilation data up to next-to-next-to-leading order accuracy. We have compared our results to existing next-to-leading order fits in the literature. The flavor singlet fragmentation function, which is known to be constrained best by data, comes out very similar as in all previous fits in both our next-to-leading and next-to-next-to-leading order analyses whereas some small ambiguities remain for the fully flavor-decomposed fragmentation functions. While the quality of our fits to electron-positron annihilation data was already acceptable at leading order accuracy, it gradually improved upon including higher-order corrections. In particular, the description of data at small momentum fractions z at the lowest energies Q is significantly better at next-to-next-to-leading order accuracy. In addition, leading order fits are found to explore regions in the parameter space which are at the border of becoming unphysical in order to achieve the best possible fit to data. As for the analysis of parton distributions, we expect global fits of fragmentation functions at next-to-next-to-leading order accuracy to become the new standard soon.

In the last part of the paper we have illustrated some salient features of the next-to-next-to-leading order corrections to the evolution of fragmentation functions and hadron production in electron-positron annihilation. The most important new asset is the found reduction of theoretical uncertainties related to the choice of the factorization scale by about a factor of 2 as compared to the next-to-leading order level. The uncertainties now match the precision of the data in most of the kinematic regime

relevant for an analysis of fragmentation functions. A similar reduction by a factor of 2 was found for the size of the genuine higher-order corrections relative to calculations performed one order lower in the perturbative series, i.e., in the K factor. The latter and the scale ambiguity tend to increase both for very large and small values of z , indicating the presence and numerical relevance of large logarithmic corrections in the perturbative series, which eventually should be resummed to all orders.

There are several avenues one can follow to further improve the theoretical framework for the analysis of fragmentation functions and the phenomenology of single-inclusive hadron production in electron-positron annihilation. First and foremost, one can include the mentioned all-order resummations, for which our code in Mellin moment space is particularly suited. This will allow one to not only extend the range in z where fits to fragmentation functions can be performed reliably but it would also give access to other experimentally relevant quantities such as integrated hadron multiplicities.

As is well known and utilized in global QCD analyses of fragmentation functions at next-to-leading order already, other processes such as semi-inclusive deep-inelastic scattering or inclusive hadron production in hadron-hadron collisions provide invaluable information on the flavor decomposition and the gluon fragmentation function. Full next-to-next-to-leading order expressions for these processes are unfortunately not yet available but one can resort to results obtained with resummation techniques that contain the dominant higher-order terms. Again, these expression can be most conveniently implemented numerically in terms of Mellin moments.

Finally, the treatment of heavy quark to light meson fragmentation functions in global analyses certainly leaves room for improvement. For instance, matching conditions for a variable flavor-number scheme are only known up to next-to-leading order accuracy so far. We plan to provide quantitative studies along all these directions in the near future.

ACKNOWLEDGMENTS

We are grateful to R. Sassot, W. Vogelsang, and A. Vogt for helpful discussions and comments. We greatly appreciate extensive discussion with the authors of the MELA code, V. Bertone, S. Carrazza, and E. R. Nocera. D. P. A. acknowledges partial support from the Fondazione Cassa Rurale di Trento. This work was supported in part by the Bundesministerium für Bildung und Forschung (BMBF) under Grant No. 05P12VTCTG and by the Institutional Strategy of the University of Tübingen (DFG, ZUK 63). This research is supported by the U.S. Department of Energy, Office of Science under Contract No. DE-AC52-06NA25396 and by the DOE Early Career Program under Grant No. 2012LANL7033.

- [1] See, e.g., J. C. Collins, D. E. Soper, and G. F. Sterman, Factorization of hard processes in QCD, *Adv. Ser. Dir. High Energy Phys.* **5**, 1 (1988).
- [2] J. C. Collins and D. E. Soper, Back-to-back jets in QCD, *Nucl. Phys.* **B193**, 381 (1981); **B213**, 545(E) (1983); Parton distribution and decay functions, *Nucl. Phys.* **B194**, 445 (1982).
- [3] S. Kretzer, Fragmentation functions from flavor inclusive and flavor tagged e^+e^- annihilations, *Phys. Rev. D* **62**, 054001 (2000).
- [4] J. Binnewies, B. A. Kniehl, and G. Kramer, Next-to-leading order fragmentation functions for pions and kaons, *Z. Phys. C* **65**, 471 (1995); B. A. Kniehl, G. Kramer, and B. Potter, Fragmentation functions for pions, kaons, and protons at next-to-leading order, *Nucl. Phys.* **B582**, 514 (2000); S. Albino, B. A. Kniehl, and G. Kramer, Fragmentation functions for light charged hadrons with complete quark flavor separation, *Nucl. Phys.* **B725**, 181 (2005); AKK update: Improvements from new theoretical input and experimental data, *Nucl. Phys.* **B803**, 42 (2008).
- [5] M. Hirai, S. Kumano, T.-H. Nagai, and K. Sudoh, Determination of fragmentation functions and their uncertainties, *Phys. Rev. D* **75**, 094009 (2007).
- [6] D. de Florian, R. Sassot, and M. Stratmann, Global analysis of fragmentation functions for pions and kaons and their uncertainties, *Phys. Rev. D* **75**, 114010 (2007).
- [7] D. de Florian, R. Sassot, and M. Stratmann, Global analysis of fragmentation functions for protons and charged hadrons, *Phys. Rev. D* **76**, 074033 (2007).
- [8] D. de Florian, R. Sassot, M. Epele, R. J. Hernandez-Pinto, and M. Stratmann, Parton-to-pion fragmentation reloaded, *Phys. Rev. D* **91**, 014035 (2015).
- [9] M. Leitgab *et al.* (Belle Collaboration), Precision Measurement of Charged Pion and Kaon Multiplicities in Electron-Positron Annihilation at $Q = 10.52$ GeV, *Phys. Rev. Lett.* **111**, 062002 (2013).
- [10] J. P. Lees *et al.* (BABAR Collaboration), Production of charged pions, kaons and protons in e^+e^- annihilations into hadrons at $\sqrt{s} = 10.54$ GeV, *Phys. Rev. D* **88**, 032011 (2013).
- [11] See, for instance, L. A. Harland-Lang, A. D. Martin, P. Motylinski, and R. S. Thorne, Parton distributions in the LHC era: MMHT 2014 PDFs, *Eur. Phys. J. C* **75**, 204 (2015); R. D. Ball *et al.* (NNPDF Collaboration), Parton distributions for the LHC Run II, *J. High Energy Phys.* **04** (2015) 040; S. Dulat *et al.*, The CT14 global analysis of quantum chromodynamics, [arXiv:1506.07443](https://arxiv.org/abs/1506.07443).
- [12] P. J. Rijken and W. L. van Neerven, $\mathcal{O}(\alpha_s^2)$ contributions to the longitudinal fragmentation function in e^+e^- annihilation, *Phys. Lett. B* **386**, 422 (1996).
- [13] P. J. Rijken and W. L. van Neerven, Higher order QCD corrections to the transverse and longitudinal fragmentation functions in electron-positron annihilation, *Nucl. Phys.* **B487**, 233 (1997).
- [14] A. Mitov and S. O. Moch, QCD Corrections to semi-inclusive hadron production in electron-positron annihilation at two loops, *Nucl. Phys.* **B751**, 18 (2006).
- [15] J. Blumlein and V. Ravindran, $\mathcal{O}(\alpha_s^2)$ timelike Wilson coefficients for parton-fragmentation functions in Mellin space, *Nucl. Phys.* **B749**, 1 (2006).
- [16] A. Mitov, S. Moch, and A. Vogt, Next-to-next-to-leading order evolution of non-singlet fragmentation functions, *Phys. Lett. B* **638**, 61 (2006); S. Moch and A. Vogt, On third-order timelike splitting functions and top-mediated Higgs decay into hadrons, *Phys. Lett. B* **659**, 290 (2008); A. A. Almasy, S. Moch, and A. Vogt, On the next-to-next-to-leading order evolution of flavour-singlet fragmentation functions, *Nucl. Phys.* **B854**, 133 (2012).
- [17] V. Bertone, S. Carrazza, and E. R. Nocera, Reference results for time-like evolution up to $\mathcal{O}(\alpha_s^3)$, *J. High Energy Phys.* **03** (2015) 46.
- [18] See, for instance, P. Nason and B. R. Webber, Scaling violation in e^+e^- fragmentation functions: QCD evolution, hadronization and heavy quark mass effects, *Nucl. Phys.* **B421**, 473 (1994).
- [19] K. G. Chetyrkin, A. L. Kataev, and F. V. Tkachov, Higher-order corrections to $\sigma_{\text{tot}}(e^+e^- \rightarrow \text{hadrons})$ in quantum chromodynamics, *Phys. Lett.* **85B**, 277 (1979); M. Dine and J. Sapirstein, Higher-Order Quantum Chromodynamic Corrections in e^+e^- Annihilation, *Phys. Rev. Lett.* **43**, 668 (1979); W. Celmaster and R. J. Gonsalves, Analytic Calculation of Higher-Order Quantum-Chromodynamic Corrections in e^+e^- Annihilation, *Phys. Rev. Lett.* **44**, 560 (1980).
- [20] S. Moch, J. A. M. Vermaseren, and A. Vogt, The longitudinal structure function at the third order, *Phys. Lett. B* **606**, 123 (2005).
- [21] G. Altarelli, R. K. Ellis, G. Martinelli, and S. Y. Pi, Processes involving fragmentation functions beyond the leading order in QCD, *Nucl. Phys.* **B160**, 301 (1979); W. Furmanski and R. Petronzio, Lepton-hadron processes beyond leading order in quantum chromodynamics, *Z. Phys. C* **11**, 293 (1982).
- [22] M. Höschele, J. Hoff, A. Pak, M. Steinhauser, and T. Ueda, MT: A Mathematica package to compute convolutions, *Comput. Phys. Commun.* **185**, 528 (2014).
- [23] D. Maitre, HPL: A Mathematica implementation of the harmonic polylogarithms, *Comput. Phys. Commun.* **174**, 222 (2006).
- [24] E. Remiddi and J. A. M. Vermaseren, Harmonic polylogarithms, *Int. J. Mod. Phys. A* **15**, 725 (2000).
- [25] E. G. Floratos, D. A. Ross, and C. T. Sachrajda, Higher order effects in asymptotically free gauge theories: The anomalous dimensions of Wilson operators, *Nucl. Phys.* **B129**, 66 (1977); *Nucl. Phys.* **B139**, 545(E) (1978); D. A. Ross and C. T. Sachrajda, Flavor symmetry breaking in anti-quark distributions, *Nucl. Phys.* **B149**, 497 (1979); G. Curci, W. Furmanski, and R. Petronzio, Evolution of parton densities beyond leading order: The nonsinglet case, *Nucl. Phys.* **B175**, 27 (1980).
- [26] J. Blumlein and S. Kurth, Harmonic sums and Mellin transforms up to two-loop order, *Phys. Rev. D* **60**, 014018 (1999).
- [27] J. Blumlein, Analytic continuation of Mellin transforms up to two loop order, *Comput. Phys. Commun.* **133**, 76 (2000).
- [28] J. Blumlein, Structural relations of harmonic sums and Mellin transforms up to weight $w = 5$, *Comput. Phys. Commun.* **180**, 2218 (2009).
- [29] S. Moch, J. A. M. Vermaseren, and A. Vogt, The three-loop splitting functions in QCD: The non-singlet case, *Nucl.*

- Phys.* **B688**, 101 (2004); A. Vogt, S. Moch, and J. A. M. Vermaseren, The three-loop splitting functions in QCD: The singlet case, *Nucl. Phys.* **B691**, 129 (2004).
- [30] O. Gituliar and S. Moch, Towards three-loop QCD corrections to the time-like splitting functions, *Acta Phys. Pol. B* **46**, 1279 (2015).
- [31] A. Vogt, Efficient evolution of unpolarized and polarized parton distributions with QCD-PEGASUS, *Comput. Phys. Commun.* **170**, 65 (2005).
- [32] S. Catani, D. de Florian, G. Rodrigo, and W. Vogelsang, Perturbative Generation of a Strange-Quark Asymmetry in the Nucleon, *Phys. Rev. Lett.* **93**, 152003 (2004).
- [33] O. V. Tarasov, A. A. Vladimirov, and A. Y. Zharkov, The Gell-Mann-Low function of QCD in the three loop approximation, *Phys. Lett.* **93B**, 429 (1980); S. A. Larin and J. A. M. Vermaseren, The three loop QCD Beta function and anomalous dimensions, *Phys. Lett. B* **303**, 334 (1993).
- [34] M. Buza, Y. Maitiounine, J. Smith, and W. L. van Neerven, Charm electroproduction viewed in the variable flavor number scheme versus fixed order perturbation theory, *Eur. Phys. J. C* **1**, 301 (1998).
- [35] S. A. Larin, T. van Ritbergen, and J. A. M. Vermaseren, The large quark mass expansion of $\Gamma(Z^0 \rightarrow \text{hadrons})$ and $\Gamma(\tau^- \rightarrow \nu_\tau + \text{hadrons})$ in the order α_s^3 , *Nucl. Phys.* **B438**, 278 (1995); K. G. Chetyrkin, B. A. Kniehl, and M. Steinhauser, Strong Coupling Constant with Flavor Thresholds at Four Loops in the Modified Minimal-Subtraction Scheme, *Phys. Rev. Lett.* **79**, 2184 (1997).
- [36] M. Cacciari, P. Nason, and C. Oleari, Crossing heavy-flavor thresholds in fragmentation functions, *J. High Energy Phys.* **10** (2005) 034.
- [37] A. H. Mueller, On the multiplicity of hadrons in QCD Jets, *Phys. Lett.* **104B**, 161 (1981); A. Bassetto, M. Ciafaloni, G. Marchesini, and A. H. Mueller, Jet multiplicity and soft gluon factorization, *Nucl. Phys.* **B207**, 189 (1982).
- [38] See, e. g., L. N. Lipatov, Small- x physics in perturbative QCD, *Phys. Rep.* **286**, 131 (1997) and references therein.
- [39] See, for example, *Handbook of Mathematical Functions*, 9th printing, edited by M. Abramowitz and I. A. Stegun (Dover, New York, 1974).
- [40] K. Abe *et al.* (SLD Collaboration), Production of π^+ , K^+ , K^0 , K^{*0} , ϕ , p and Λ^0 in hadronic Z^0 decays, *Phys. Rev. D* **59**, 052001 (1999).
- [41] D. Buskulic *et al.* (Aleph Collaboration), Inclusive π^\pm , K^\pm and (p, \bar{p}) differential cross-sections at the Z resonance, *Z. Phys. C* **66**, 355 (1995).
- [42] P. Abreu *et al.* (Delphi Collaboration), π^\pm , K^\pm , p and \bar{p} production in $Z^0 \rightarrow q\bar{q}$, $Z^0 \rightarrow b\bar{b}$, $Z^0 \rightarrow u\bar{u}$, $d\bar{d}$, $s\bar{s}$, *Eur. Phys. J. C* **5**, 585 (1998).
- [43] R. Akers *et al.* (Opal Collaboration), Measurement of the production rates of charged hadrons in e^+e^- annihilation at the Z^0 , *Z. Phys. C* **63**, 181 (1994).
- [44] H. Aihara *et al.* (TPC/Two Gamma Collaboration), Pion and kaon multiplicities in heavy quark jets from e^+e^- annihilation at 29-GeV, *Phys. Lett. B* **184**, 299 (1987); Charged Hadron Inclusive Cross Sections and Fractions in e^+e^- Annihilation at $\sqrt{s} = 29$ GeV, *Phys. Rev. Lett.* **61**, 1263 (1988); X.-Q. Lu, Ph.D. thesis, Johns Hopkins University, 1987 [Report No. UMI-87-07273].
- [45] A. Accardi, D. P. Anderle, and F. Ringer, Interplay of threshold resummation and hadron mass corrections in deep inelastic processes, *Phys. Rev. D* **91**, 034008 (2015).
- [46] A. H. Mueller, Multiplicity and hadron distributions in QCD Jets: Nonleading terms, *Nucl. Phys.* **B213**, 85 (1983); Square root of $\alpha(Q^2)$ corrections to particle multiplicity ratios in gluon and quark jets, *Nucl. Phys.* **B241**, 141 (1984); J. B. Gaffney and A. H. Mueller, $\alpha(Q^2)$ corrections to particle multiplicity ratios in gluon and quark jets, *Nucl. Phys.* **B250**, 109 (1985).
- [47] For some recent work, see, A. Vogt, Resummation of small- x double logarithms in QCD: Semi-inclusive electron-positron annihilation, *J. High Energy Phys.* **10** (2011) 025; S. Albino, P. Bolzoni, B. A. Kniehl, and A. Kotikov, Fully double-logarithm-resummed cross sections, *Nucl. Phys.* **B851**, 86 (2011); Timelike single-logarithm-resummed splitting functions, *Nucl. Phys.* **B855**, 801 (2012); C.-H. Kom, A. Vogt, and K. Yeats, Resummed small- x and first-moment evolution of fragmentation functions in perturbative QCD, *J. High Energy Phys.* **10** (2012) 033.
- [48] M. Cacciari and S. Catani, Soft gluon resummation for the fragmentation of light and heavy quarks at large x , *Nucl. Phys.* **B617**, 253 (2001); J. Blumlein and V. Ravindran, QCD threshold corrections to Higgs decay and to hadroproduction in 1^+1^- annihilation, *Phys. Lett. B* **640**, 40 (2006); S. Moch and A. Vogt, Higher-order threshold resummation for semi-inclusive e^+e^- annihilation, *Phys. Lett. B* **680**, 239 (2009); D. P. Anderle, F. Ringer, and W. Vogelsang, QCD resummation for semi-inclusive hadron production processes, *Phys. Rev. D* **87**, 034014 (2013).